Preparation and characterization of slurry for chemical mechanical planarization (CMP)

11

J. Seo, U. Paik
Hanyang University, Seoul, South Korea

11.1 Introduction

Since chemical mechanical planarization (CMP) was developed in the 1980s at IBM, it has played a key role for integrated circuit (IC) manufacturing (Beyer, 1999). In the IC fabrication process, front-end-of-line (FEOL) and back-end-of-line (BEOL) processes have been crucial applications of CMP (Krishnan et al., 2009). FEOL CMP is the process that forms the shallow trench isolation (STI) by polishing the gap-filling materials such as SiO_2. BEOL CMP is used to form metal interconnects including Al, W, and Cu. In general, CMP slurries are composed of abrasive, oxidizer, organic compounds such as dispersant and passivation agent, and deionized water (DIW). Specific slurry formulations are different depending on the materials to be polished. The physicochemical properties of slurry that have significant influence on CMP performances are determined by the complex interactions between its components. As the design rule is reduced, the demands on CMP performance have become more stringent. Thus, understanding the physicochemical properties of slurry is essential to develop CMP slurries for next-generation devices including new materials and complex structures.

11.2 Preparation of slurry for CMP

The CMP process can be divided into interlayer dielectric (ILD) CMP, STI CMP, and metal (W, Cu, and Al) CMP. ILD CMP is a process that polishes dielectric materials such as SiO_2 deposited between metal interconnects. Slurries are composed of abrasive, dispersant, and other additives. STI CMP is a process that uniformly polishes the step height of SiO_2, formed by the gap-filling process, and stop on stopping layer such as the Si_3N_4 or poly-silicon (poly-Si) film. There are requirements on the high polish rate selectivity between SiO_2 and stopping materials to prevent their erosion. For this reason, slurries for STI CMP contain passivation agents for high selectivity.

Contrary to ILD and STI CMP, metal films are hard to remove using abrasives because of their inertness. Thus, metal CMP slurries need suitable oxidizers to form an oxidation layer on the surface that can be easily removed by abrasives.

Advances in Chemical Mechanical Planarization (CMP). http://dx.doi.org/10.1016/B978-0-08-100165-3.00011-5

To formulate these slurries that are suitable for each CMP process, it is very important to understand the role and characteristics of each component in slurries. In this section, we will discuss the role and characteristics of each component for CMP performances in detail.

11.2.1 Abrasive particles

Abrasive particles are one of the main components in CMP slurry. Silica, ceria, alumina, and other materials have been used as abrasives. Silica abrasives have been widely used for ILD, STI CMP, and metal CMP. There are two types of silica abrasives: fumed and colloidal silica. Figure 11.1 shows their transmission electron microscopy (TEM) images (Zhang et al., 2012). Fumed silica, made from flame pyrolysis of silicon tetrachloride ($SiCl_4 + 2H_2O \rightarrow SiO_2 + 4HCl$), has been used as an abrasive because of its inexpensive price, high purity, and simple synthesis. However, it forms a network structure in an aqueous media caused by weak hydrogen bonding, resulting in agglomeration. Thus, subsequent processes such as microfluidizer treatment and filtration process are essential to formulate CMP slurries using fumed silica. Contrary to fumed silica, colloidal silica can be made with the desired particle size and uniform size distribution through hydrolysis of metal organic precursors (by the net reaction $\equiv Si{-}OH + HO{-}Si\equiv \leftrightarrow \equiv Si{-}O{-}Si\equiv$). Silicic acid sodium and organic silicate are used as precursors to prepare colloidal silica. Colloidal silica, made from silicic acid sodium, inevitably contains large amounts of sodium ions, which can cause severe problems such as damage on the gate oxides of a device. In order to use it, the ion-exchange process is required to remove sodium ions. Organic silicate can produce high purity silica compared with silicic acid sodium, and be used as an abrasive for polishing after the washing and decant process to remove residual precursors. The demands on defect become more stringent with a decrease in device dimensions. Thus, fumed silica has recently been replaced by colloidal silica in CMP processes that require high surface quality of polished film.

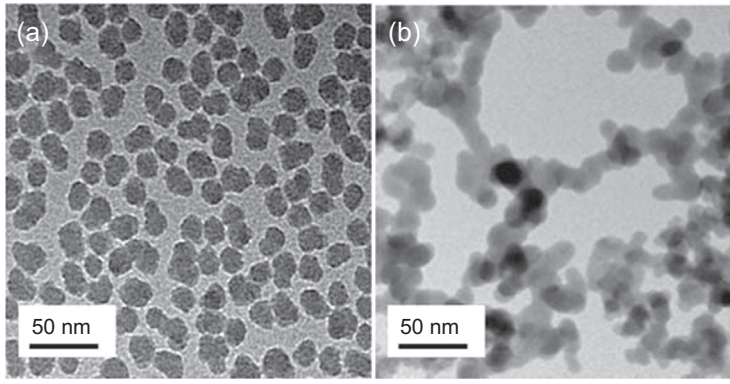

Figure 11.1 TEM images of (a) colloidal silica and (b) fumed silica nanoparticle aggregates. Zhang et al. (2012).

Ceria has been used as an abrasive for ILD and STI CMP because of its high SiO_2 removal rate (RR). It can form strong Ce−O−Si bonding during SiO_2 polishing, leading to a high SiO_2 RR (Cook, 1990).

$$-\mathrm{Ce}-\mathrm{OH} + -\mathrm{Si}-\mathrm{O}^- \leftrightarrow -\mathrm{Ce}-\mathrm{O}-\mathrm{Si}- + \mathrm{OH}^- \tag{11.1}$$

Ceria abrasives show higher surface quality and selectivity as well as higher RRs of SiO_2 than silica abrasives. Thus, as an abrasive for SiO_2 CMP, silica is being replaced by ceria. Figure 11.2 shows TEM images of ceria synthesized through the solid-state and solution-grown method (Seo et al., 2014). The solid-state method produces ceria abrasives with a controllable crystallite size depending on synthesis conditions (Kim et al., 2003). However, it has not only large particle size and poor size distribution, but also an angulated shape (Figure 11.2(a)). Thus, mechanical milling and filtration processes are essential to obtain the desired particle size and uniform size distribution (Kim et al., 2006). Compared with the solid-state method, the solution-grown method produces spherical ceria abrasives with the desired particle size and uniform size distribution (Figure 11.2(b)). These characteristics of the solution-grown ceria lead to low defects during CMP. Recently, many researchers have studied the physicochemical properties of solution-grown ceria to develop defect-free CMP slurries. In Section 11.3.3, we will discuss the physicochemical properties of solution-grown ceria in detail.

As an abrasive for metal CMP, alumina has been used because of high polish rate selectivity between metal (W or Cu) and a barrier metal (Ti/TiN or Ta/TaN) (Krishnan et al., 2009). Alumina abrasive can exist in various phases (α, β, γ, or δ) depending on the calcination temperature. However, it commonly generates many defects during polishing because of its hardness. There have been several studies to overcome these limitations (Lei and Zhang, 2007; Zhang and Lei, 2008). Lei and Zhang developed the alumina/silica core−shell abrasive for polishing hard disk substrates. Zhang and Lei reported alumina composite abrasive grafted with polymethacrylic acid for glass polishing. These composite abrasives show improved surface planarization and fewer scratches than pure alumina abrasives because of the cushioning effect of their

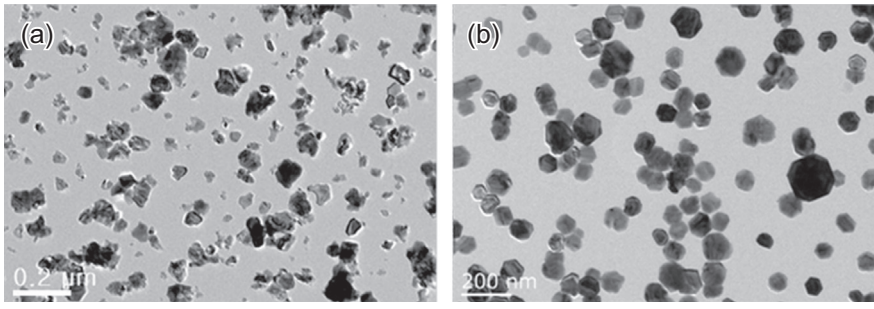

Figure 11.2 TEM images of (a) solid-state ceria and (b) solution-grown ceria.
Seo et al. (2014).

structure. For this reason, alumina abrasives have been used as the composite structure rather than in pure form.

11.2.2 Dispersants

Dispersants are widely used to improve dispersion stability. According to the DLVO (Derjaguin, Landau, Vervey, and Overbeek) theory, particles in aqueous media can be agglomerated when van der Waals attraction is greater than electrostatic repulsion (Verwey et al., 1999; Derjaguin and Landau, 1941). By adding suitable dispersants, steric hindrance and electrostatic stabilization between the abrasives are obtained, which prevent abrasives from agglomerating.

Generally, abrasive particles in slurry are known to undergo transitions from bridging agglomeration → stable → depletion flocculation with an increase in dispersant concentration (Kim et al., 2012). At a low concentration, dispersants are insufficient for full coverage of the abrasive surface. The free segments (loops and tails) of the adsorbed dispersant on the abrasive surface can attach to other abrasives, leading to bridging agglomeration. When an adequate amount of dispersant is added, it fully covers the abrasive surface, which can improve the dispersion stability through steric hindrance and electrostatic stabilization. Also, dispersants should have strong adsorption energy with the abrasive surface. Weak adsorption energy between dispersant and abrasive surface causes desorption of the dispersant during a particle collision, resulting in bridging flocculation (Sigmund et al., 2000). At a high concentration of dispersants, free dispersants (not adsorbed) can promote flocculation of the stable slurry through a depletion mechanism (Asakura and Oosawa, 1954, 1958). When two particle surfaces approach each other at a distance less than the effective diameter of unabsorbed dispersants, the dispersants are excluded from the interparticle gap, resulting in an osmotic pressure. This osmotic pressure generates an attractive force between the abrasive particles, which promotes their flocculation. Thus, it is important to add an adequate amount of dispersants for improved dispersion stability.

Langmuir and Freundlich adsorption models can be used to describe the adsorption behavior of dispersants on an abrasive surface. The Langmuir adsorption isotherm model assumes that the particle surface is homogeneously covered by the monolayer dispersant. It is expressed as follows:

$$C_e/Q_e = C_e/Q_m + 1/(K_L Q_m) \tag{11.2}$$

where Q_e is the adsorbed amount of dispersant per surface area of particle at equilibrium (mg/m^2), C_e is the concentration of dispersant in the bulk solution (mg/L), Q_m is the maximum adsorbed amount of dispersant on particle surface (mg/m^2), and K_L is related to the affinity of adsorption (L/mg). The Freundlich adsorption isotherm model below is used in heterogeneous systems:

$$Q_e = K_F C_e^{1/n} \tag{11.3}$$

The Freundlich constant K_F and $1/n$ are constants dependent on the relative adsorption capacity and intensity of adsorption, respectively. The values of K_F and $1/n$ are determined from the intercept and slope of a linear plot of log Q_e versus log C_e.

$$\log Q_e = \log K_F + 1/n \log C_e \tag{11.4}$$

A smaller value of $1/n$ indicates a stronger bond between dispersant and particle surface. To identify the adsorption behavior of dispersant, data are fitted with Langmuir and Freundlich adsorption models, and the adsorption model with a higher correlation coefficient values is chosen.

Figure 11.3 shows the adsorption isotherm of poly(acrylic acid) (PAA) on a ceria surface. The Langmuir adsorption model ($R^2 = 0.99$) is a much better fit than the Freundlich adsorption model ($R^2 = 0.87$), which indicates that PAA covers the ceria surface homogeneously.

To disperse abrasive particles that are used for CMP application, several dispersants have been investigated. Surfactants such as cetrimonium bromide (CTAB) and sodium dodecyl sulfate (SDS) have been investigated for silica slurries (Bu and Moudgil, 2007; Basim et al., 2003). Basim et al. reported that adsorbed CTAB on the silica abrasive provides a strong repulsive force between abrasives, leading to stable slurry (Basim et al., 2003). However, it also prevents direct contact between silica abrasives and the oxide film, resulting in a decrease in the friction force during polishing (Figure 11.4). Since the removal of material by silica abrasive is mechanically dominant, the decrease in the friction force inevitably leads to a lower material RR (MRR).

Various dispersants have been used to disperse ceria abrasive in aqueous media. PAA has been widely used to disperse ceria abrasive in CMP (Sehgal et al., 2005;

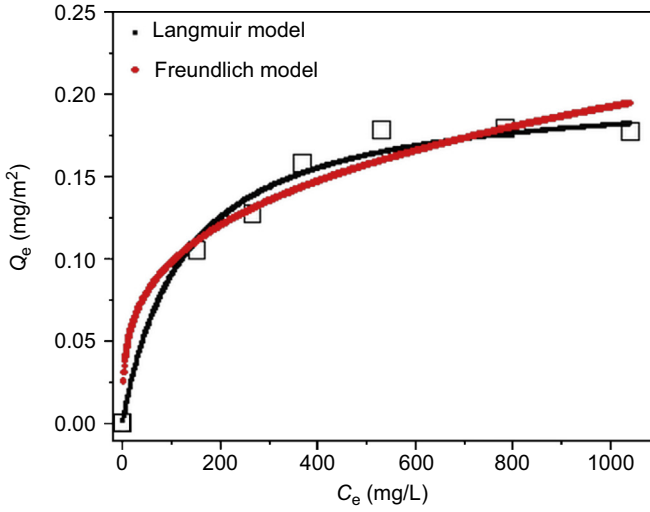

Figure 11.3 Langmuir and Freundlich plot adsorption isotherm of PAA on ceria surface.

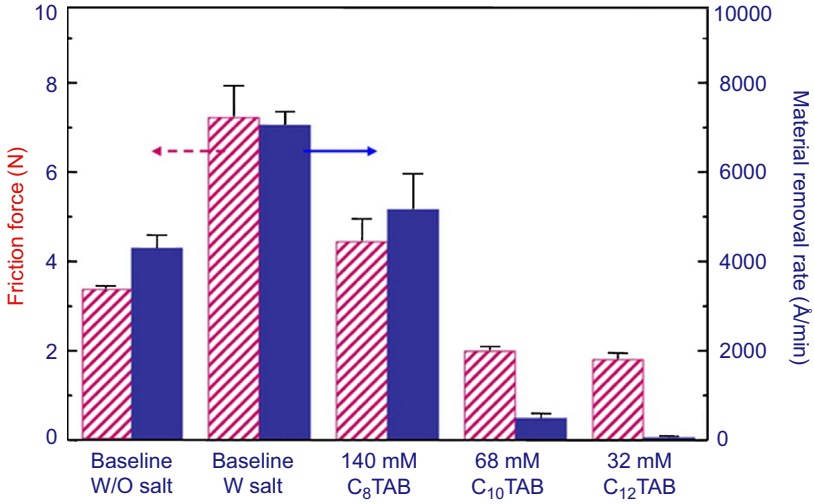

Figure 11.4 In situ friction force and material removal rate responses of the baseline slurries (12 wt%, 2.0 μm primary particle size) and the slurries containing various concentration of CTAB in the presence of 0.6 M NaCl at pH 10.5.
Basim et al. (2003).

Pettersson et al., 2000). PAA, an anionic surfactant, can adsorb on the highly positively charged ceria surface by the attractive electrostatic force. Carboxylic (−COOH) groups of PAA adsorbed on the ceria surface are deprotonated to negatively charged carboxylate ($-COO^-$) groups above their pK_a of 4.5, which improves the dispersion stability through an increase in repulsive force between abrasives. The ceria abrasives chemically remove the materials through interaction between active sites on surface and film whereas silica abrasives mechanically remove the material (Wang et al., 2007; Dandu et al., 2011). For this reason, a significant decrease in MRR is not observed because of the PAA adsorbed on the abrasive surface. Kim et al. proposed that the coadsorption of poly(methyl methacrylate) and hydrogen citrate on the ceria surface can increase the repulsive force between abrasives, which improves dispersion stability (Kim et al., 2010). Figure 11.5 shows SiO_2 MRR and within-wafer nonuniformity (WIWNU) during STI CMP. The results show that the improved dispersion stability leads to an increase in SiO_2 MRR and improved uniformity. Also, the number of residual abrasive particles is significantly decreased because of the increase in repulsive force between the abrasives and the film.

There are several reports that show highly active Ce^{3+} on a ceria surface has influence on SiO_2 MRR (Dandu et al., 2010; Kelsall, 1998). Dandu et al. identified through UV-visible spectroscopy that several additives (arginine, ornithine, and lysine) can interact with Ce^{3+} on the ceria surface (Dandu et al., 2010, 2011). These additives can block the Ce^{3+} on the abrasive surface by forming Ce−O−Si bondings during SiO_2 polishing, leading to a significant decrease in MRR. Thus, dispersants should be chosen by considering their chemical interaction with abrasives.

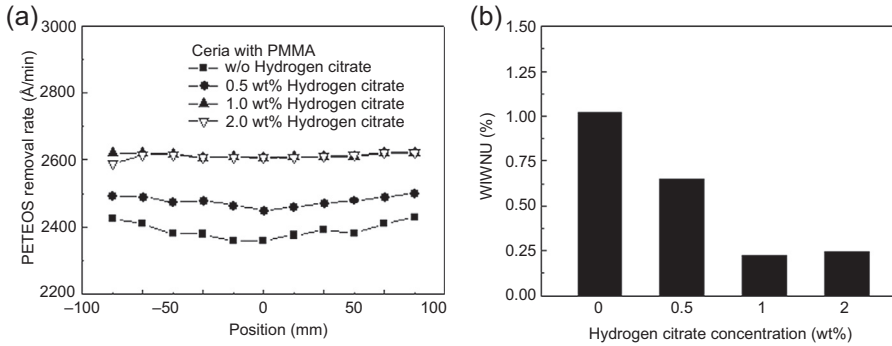

Figure 11.5 (a) Removal rate trends along radius of SiO_2 film and (b) WIWNU of SiO_2 film on STI CMP field evaluation.
Kim et al. (2010).

11.2.3 Passivation agents for high selectivity

Passivation agents are used for selective removal of a specific material among various materials during CMP. In STI CMP, polishing is stopped on the Si_3N_4 film after the step height structure of SiO_2 is planarized. In the absence of passivation agents, erosion of Si_3N_4 film, which has a direct influence on device yield, can occur. Generally, an anionic surfactant such as PAA has been widely used as a passivation agent for obtaining high polish rate selectivity between SiO_2 and Si_3N_4 (Park et al., 2003; Kim et al., 2008). PAA can preferentially absorb on the highly positively charged Si_3N_4 surface through the attractive electrostatic force (Hackley, 1997). This PAA adsorption layer prevents the abrasive from polishing the Si_3N_4 film, resulting in high polish rate selectivity between SiO_2 and Si_3N_4. Kim et al. controlled the conformation of adsorbed PAA on the Si_3N_4 film with the addition of KNO_3 (Kim et al., 2008). As shown in Figure 11.6, they observed that the adsorbed PAA layer on Si_3N_4 film is denser with an increase in KNO_3 concentration. It is attributed to the charge screening of PAA by potassium ions. The densely adsorbed PAA layer on Si_3N_4 film, formed at high ionic strength, prevents the ceria abrasives from polishing the Si_3N_4 film, which decreases the RR of Si_3N_4 film from 72 to 61 Å/min, resulting in increased polishing rate selectivity between SiO_2 and Si_3N_4.

Penta et al. investigated four anionic surfactants with different functional groups as passivation agents for high selectivity in STI CMP (Penta et al., 2013a). Figure 11.7 shows the RRs of SiO_2 and Si_3N_4 in the presence of four different anionic surfactants. All anionic surfactants can form the bilayer on Si_3N_4 film below the isoelectric point of Si_3N_4. A monolayer is formed through electrostatic interaction between SiO_2 and Si_3N_4, followed by a secondary layer through hydrophobic interaction between the surfactant tails. These adsorption layers suppress the Si_3N_4 MRR during polishing, leading to high polishing rate selectivity between SiO_2 and Si_3N_4. Contrary to these surfactants, the ionic salt K_2SO_4 adsorbs only weakly on the Si_3N_4 film, and cannot suppress the Si_3N_4 MRR.

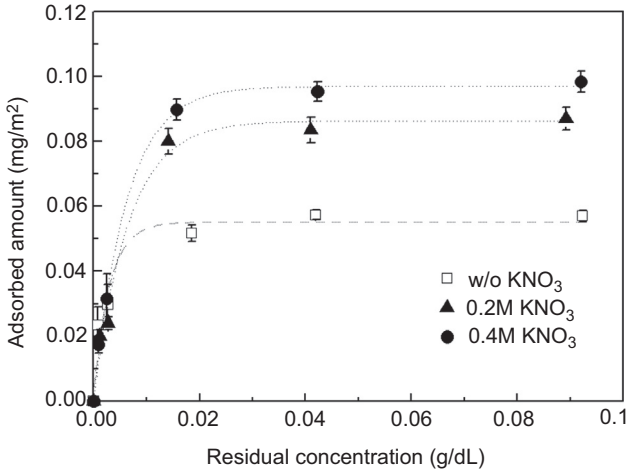

Figure 11.6 Adsorption isotherms for PAA as a function of ionic strength on Si_3N_4 at pH 6.5. Kim et al. (2008).

Recently, various amino acids also have been investigated as passivation agents in STI CMP (Penta et al., 2013b; Veera et al., 2009). Penta et al. reported that amino acids, having both an amine group and a carboxyl group, can suppress the removal of Si_3N_4 through formation of a hydrogen bond between the protonated amino group of the amino acid and the nitrogen atoms on the Si_3N_4. The adsorption of amino acids on the Si_3N_4 can prevent the hydrolysis of the Si_3N_4. The removal of Si_3N_4 is significantly suppressed. In contrast with the Si_3N_4 film, amino acids on the SiO_2 film are weakly bound, and it can be easily removed by abrasives during polishing. As a result, the high polishing rate selectivity between SiO_2 and Si_3N_4 is shown. Since these amino acids are sensitive to a change of pH, they exhibit an "on/off" behavior on the Si_3N_4 passivation as a function of pH. These characteristics of amino acids can be applied to formulate CMP slurries for next-generation devices that include new materials and complex structures.

In NAND flash memory beyond 60 nm, the self-aligned poly-Si floating gates are constructed without the deposition of Si_3N_4. Thus, polishing rate selectivity between SiO_2 and poly-Si plays a key role in STI CMP for NAND flash. Hydrophobic surfactants that can preferentially adsorb on poly-Si film have been investigated as passivation agents for achieving high selectivity between SiO_2 and poly-Si. The selectivity can be controlled through their different surface energies. Poly-Si film has a lower surface energy than an SiO_2 film, and this difference enables preferential adsorption of passivation agents on poly-Si film. This passivation layer prevents the abrasive from polishing poly-Si film, resulting in high polish rate selectivity. Lee et al. studied the effects of various nonionic surfactants on selectivity between SiO_2 and poly-Si in STI CMP for NAND flash (Lee et al., 2002). As shown in Figure 11.8, they reported that the selectivity between SiO_2 and poly-Si is significantly correlated

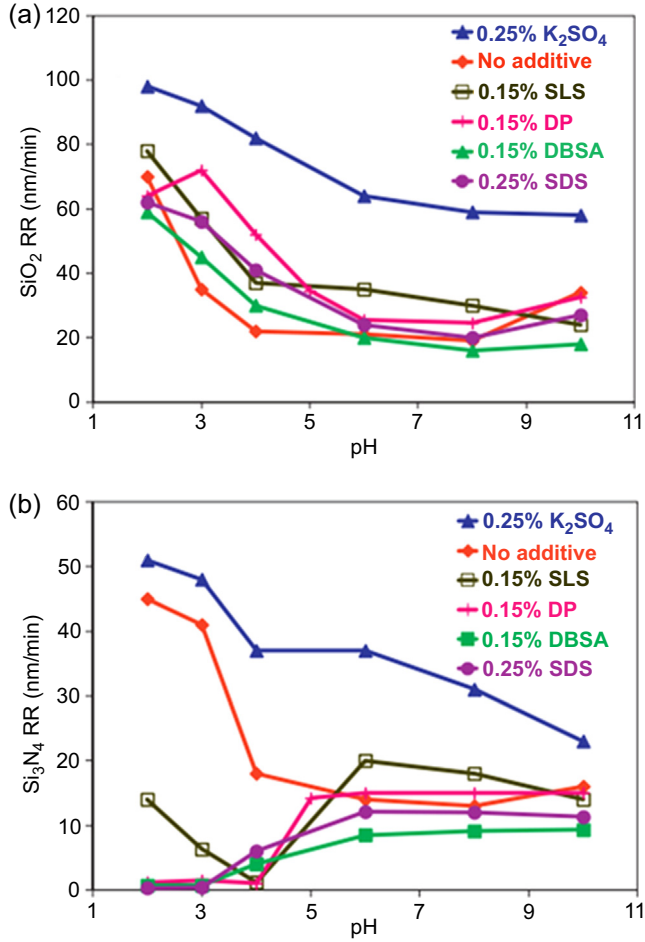

Figure 11.7 Removal rates of (a) SiO_2 and (b) Si_3N_4 with addition of anionic surfactants. Penta et al. (2013a).

with the 1/HLB (hydrophile−lipophile balance) value and molecular weight of surfactant. Also, CMP slurries containing the nonionic surfactants show a fourfold decrease in WIWNU compared to the conventional oxide slurry.

11.2.4 Oxidizers

During polishing, metal films are hard to remove by abrasive because of their inertness and hardness. With the addition of a suitable oxidizer, a metal can form an oxide layer on its surface, which can be easily removed during CMP. Since Kaufman et al. first proposed a model of the W CMP process using $K_3(Fe(CN)_6)$ (Kaufman et al., 1991), there have been studies on metal slurries containing various oxidizers

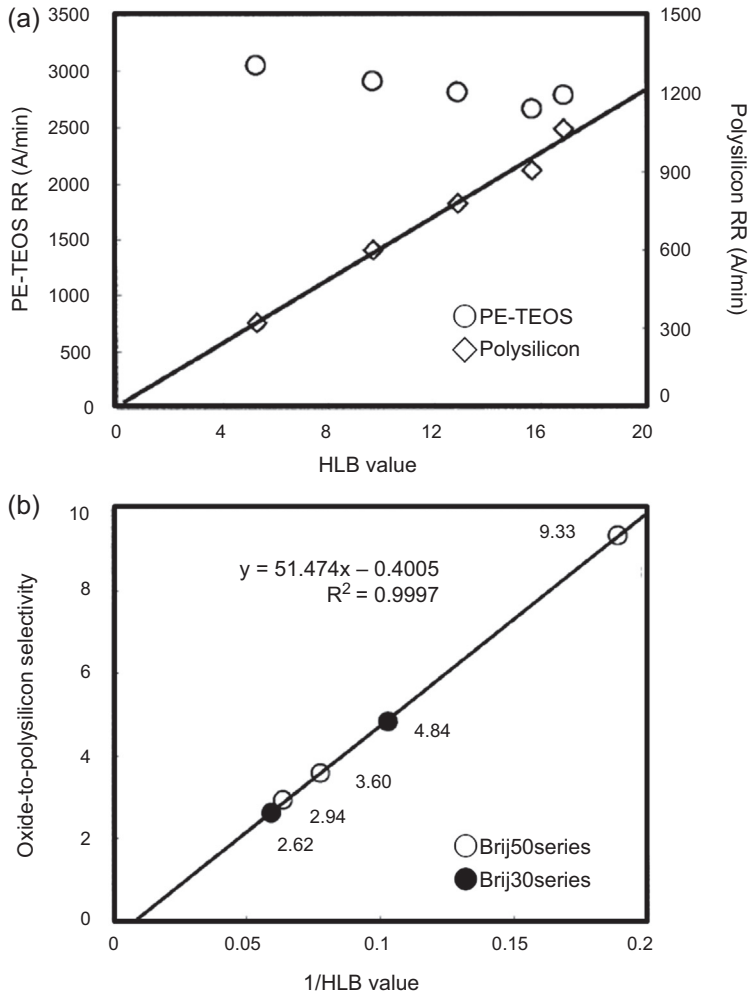

Figure 11.8 Removal rates and SiO_2-to-poly-Si selectivity as a function of HLB value of the added Brij surfactant: (a) SiO_2 and poly-Si removal rate dependency on the HLB value; (b) SiO_2 and poly-Si selectivity dependency on the 1/HLB value.
Lee et al. (2002).

(KIO_3, $Fe(NO_3)_3$, H_2O_2, organic acids, and their mixtures). In general, hydrogen peroxide (H_2O_2) has been widely used as the oxidizer for commercial metal slurries because of its low cost and powerful oxidizing capability. However, it can form a thick and porous oxide layer with poor surface quality caused by the dissolution and oxidation reactions of W (Lim et al., 2013).

Fe ions catalyze the decomposition of H_2O_2 into the hydroxyl radicals (•OH), powerful oxidants, through the Fenton reaction. These radicals can rapidly form a dense oxidation layer on the W film, resulting in high MRR and improved topography of W film. Figure 11.9 shows potentiodynamic polarization curves of W film in the

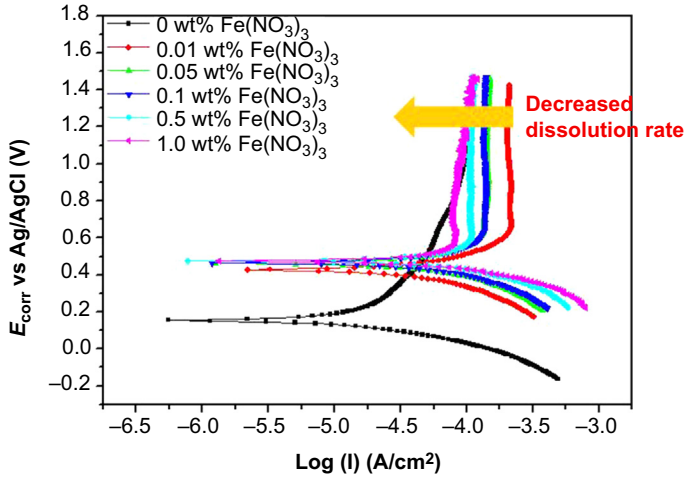

Figure 11.9 Potentiodynamic polarization curves of W film surface in the presence of 1 wt% H_2O_2 solutions at pH 2.3 with various $Fe(NO_3)_3$ concentrations.
Lim et al. (2013).

presence of 1 wt% H_2O_2 as a function of $Fe(NO_3)_3$ concentration (Lim et al., 2013). The polarization curve of W film in the absence of $Fe(NO_3)_3$ shows active corrosion behavior because the oxidation layer formed on W film is thin. However, with the addition of $Fe(NO_3)_3$, the polarization curves of W film show anodic oxidation behavior. With an increase in $Fe(NO_3)_3$ concentrations, current density is shifted to a lower value. It means that the dissolution of the W film is reduced as a result of the formation of a denser oxidation layer.

Various metal salts (Al, Ru, Ce, Co, Mn, Cu, and Cr), which have multiple redox states, also decompose H_2O_2 into ·OH through a Fenton-like reaction (Bokare and Choi, 2014). However, Fe ions have generally been used as a catalyst to decompose H_2O_2 into ·OH because of (1) high abundance, (2) an environmentally friendly nature, (3) low toxicity, (4) a highly reactive redox cycle between Fe^{2+} and Fe^{3+}, and (5) low cost.

Recently, CMP slurries for inactive materials such as ruthenium (Ru) and silicon carbide (SiC) have been proposed for new applications (Cui et al., 2013; Kurokawa et al., 2013). Several researchers are studying various oxidizers for inactive materials CMP. Cui et al. reported that Ru has a remarkable MRR with $NaIO_4$ and NaClO because of the appropriate energy barrier between the Ru/RuO_2 film and the oxidizer. Kurokawa et al. found that a mixture of N_2 and O_2 gases as well as $KMnO_4$ can increase SiC MRR. In conclusion, choice of suitable oxidizers is very important to achieve the improved CMP performances such as high MRR, high selectivity, uniformity, and low defects.

11.2.5 Inhibitors

In order to obtain the high MRR, several CMP processes may be performed under high dissolution rate of metal film. However, they inevitably lead to problems such as poor surface quality, generation of pits, and high localized etching. To solve these problems

in Cu CMP, benzotriazole (BTA) or its several derivatives have been used as a corrosion inhibitor (Ein-Eli et al., 2003; Du et al., 2004). Notoya et al. studied the formation of various Cu−BTA complexes depending on the pH (Notoya and Poling, 1976). They reported the highest corrosion inhibition of Cu at pH 6. At acidic pH, BTA exists as a protonated species, making it difficult to form the complexes with positively charged Cu film because of the repulsive force. Above pH 6, highly soluble Cu^{2+} ions can be precipitated in the form of $Cu(OH)_2$ and others.

Surfactants such as CTAB, ammonium dodecyl sulfate, and SDS were also investigated as corrosion inhibitors for Cu film. However, these surfactants may cause poor slurry stability and insufficient corrosion inhibition. Among various corrosion inhibitors reported in the literature, BTA is still the most efficient corrosion inhibitor. Although an addition of a corrosion inhibitor causes a decrease in MRR by preventing the dissolution of Cu film, it is one of essential components of high planarization and improved surface quality.

11.3 Characterizations of slurry for CMP

The characteristics of slurry such as abrasive particle size and distribution, surface chemistry, dispersion stability, and rheological behavior are determined by the complex interaction between its components, and have significant influence on CMP performances.

Among various characteristics of the slurry, abrasive particle size has significant influence on MRR. There are two models, contact area model and indentation volume model, to explain it. At the small abrasive particle, the contact area model is dominant. As abrasive size increases, the indentation volume model becomes more appropriate (Basim et al., 2000). According to Cook's hypothesis, the active sites on the abrasive surface also play a key role in MRR. These active sites are influenced by various physicochemical conditions including pH, ionic strength, temperature, and concentration. Rheological behavior of CMP slurries is also important because their mass transport on the pad can effect three-body (slurry−pad−wafer) interaction. Hence, it is very important to understand the characteristics of slurry because they have significant influence on CMP performances.

11.3.1 Abrasive characteristics: size and concentration

Abrasives in the size range 30−300 nm (aggregated size) have been used for polishing. However, the effect of abrasive size on CMP performance remains contradictory (Figure 11.10). Bielmann et al. reported that the removal mechanism of W film is related to the contact area between abrasive and wafer. As shown in Figure 11.10(a), the W MRR is increased with a decrease in abrasive size (Bielmann et al., 1999). MRR based on the contact area model is expressed as follows (Basim et al., 2000):

$$\mathrm{MRR} \propto \left(A \propto C_0^{1/3} \cdot \Phi^{-1/3} \right) \tag{11.5}$$

where A is the total contact area between abrasive and film, C_0 is the concentration of abrasive, and Φ is the abrasive diameter. When the CMP conditions and solid concentration are fixed, the MRR is increased with a decrease in abrasive size.

However, others suggest the opposite conclusions (Tamboli et al., 2004; Lei and Luo, 2004). Tamboli et al. suggested that the MRR is increased with an increase in abrasive size in CMP for tantalum and tetra-ethyl ortho-silicate (Tamboli et al., 2004). As shown in Figure 11.10(b), Lei et al. also showed that larger abrasive size leads to an increase in MRR for polishing hard disk substrate

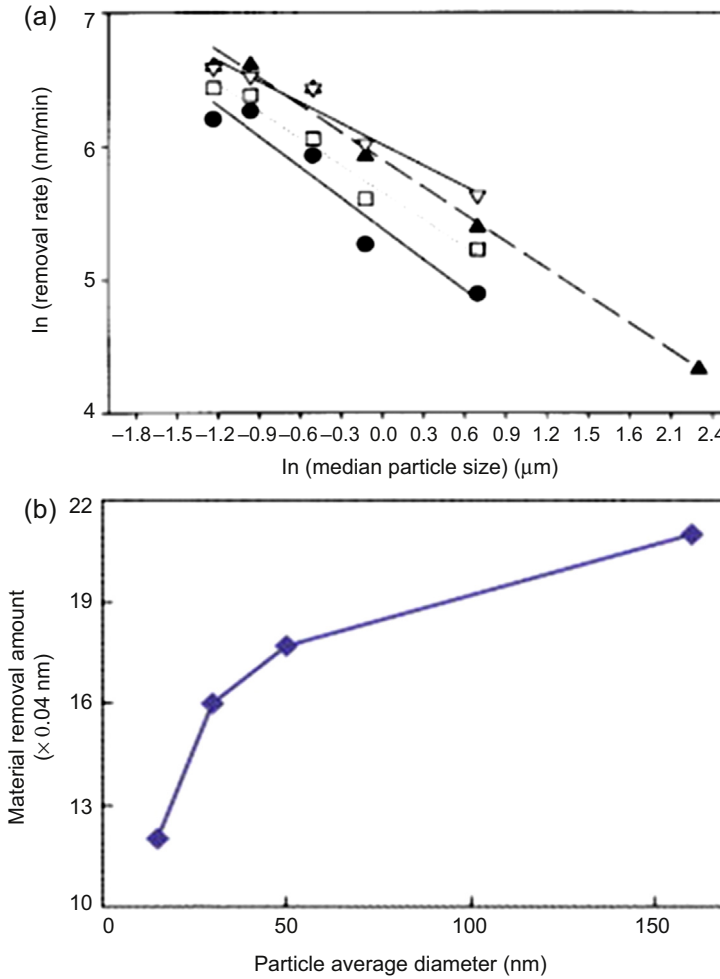

Figure 11.10 Effect of the particle size on MRR: (a) W MRR as a function of particle size for different solids loading (Bielmann et al., 1999); (b) MRR for hard disk substrate as a function of particle diameter (Lei and Luo, 2004).

(Lei and Luo, 2004). At larger abrasive sizes, the indentation volume model becomes more appropriate:

$$\mathrm{MRR} \propto \left(V \propto C_0^{-1/3} \cdot \Phi^{4/3} \right) \tag{11.6}$$

where V is the indentation volume of an abrasive particle into the wafer. The indentation volume of an abrasive particle into the wafer becomes larger because of an increase in abrasive size, which can increase the MRR.

These opposite conclusions are because slurry formulation and material removal mechanisms are different depending on the types of materials to be polished. In any case, the large abrasive sizes can produce the scratch defects on films during CMP (Remsen et al., 2005, 2006). Since the number of maximum permissible defects is continually lowered with decreasing device dimensions, CMP slurries containing smaller abrasive sizes have been investigated.

The concentrations as well as the size of the abrasives have an effect on MRR. There are three distinct regions of MRR dependence on abrasive concentration (Lee et al., 2009; Luo and Dornfeld, 2003) (Figure 11.11). First, MRR rapidly increases with an increase in abrasive concentration, which indicates that chemical removal of material is dominant at low concentrations. Second, as mechanical removal becomes dominant, MRR is proportional to the abrasive concentration. And third, the dominant mechanical effect is saturated because the contact area between abrasive and the wafer surface is at a maximum. Although the MRR varied with the abrasive concentration depending on the types of abrasives, films, and additives, their trends are quite similar. In practice, the silica slurries have high solids contents of 5−50 wt% whereas the ceria and alumina slurries have low solid contents (∼5 wt%).

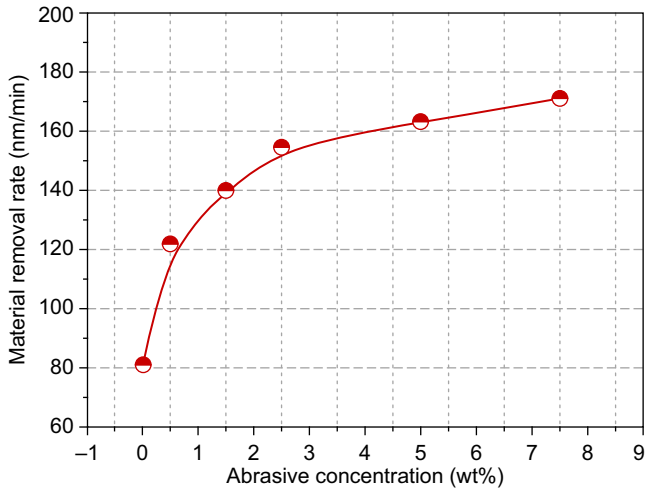

Figure 11.11 MRR as a function of abrasive concentration.
Lee et al. (2009).

11.3.2 Surface charge

Abrasives in an aqueous medium produce an interfacial charge at the solid−liquid interface through adsorption or desorption of hydrogen ions or ionic species on the abrasive surface.

$$-\mathrm{M}-\mathrm{OH} + \mathrm{H}^{+} \leftrightarrow -\mathrm{M}-\mathrm{OH}_2{}^{+} (\mathrm{pH} < \mathrm{pH}_{\mathrm{pzc}}) \tag{11.7}$$

$$-\mathrm{M}-\mathrm{OH} \leftrightarrow -\mathrm{M}-\mathrm{O}^{-} + \mathrm{H}^{+} (\mathrm{pH} > \mathrm{pH}_{\mathrm{pzc}}) \tag{11.8}$$

The point of zero charge (pzc) is the pH value when the numbers of $[-\mathrm{M}-\mathrm{OH}_2^{+}]$ and $[-\mathrm{M}-\mathrm{O}^{-}]$ are equal. At the $\mathrm{pH}_{\mathrm{pzc}}$, abrasive particles show zero zeta potential. This insufficient surface charge between abrasive particles decreases the energy barrier for agglomeration, resulting in poor dispersion stability. Thus, it has to be formulated at $\mathrm{pH} < \mathrm{pH}_{\mathrm{pzc}}$ or $\mathrm{pH} > \mathrm{pH}_{\mathrm{pzc}}$ where abrasive particles have a highly charged surface.

Figure 11.12 shows the electrokinetic behaviors of materials used in STI CMP (Kim et al., 2003). The surface potentials of all materials are strongly dependent on the suspension pH. The SiO_2 shows negative charge above $\mathrm{pH}_{\mathrm{pzc}}$ 3. Its charge is slightly decreased with an increase in pH above pH 9, which is attributed to the compression of the electrical double layer by dissolved Si ions (Paik et al., 2001). Si_3N_4 shows a negative charge above $\mathrm{pH}_{\mathrm{pzc}}$ 6.5 by the formation of SiO^{-}. In the pH range 3−6.5, SiO_2 and Si_3N_4 films show different surface charge. These different surface potentials enable the passivation agent to preferentially adsorb on the Si_3N_4 film, resulting in

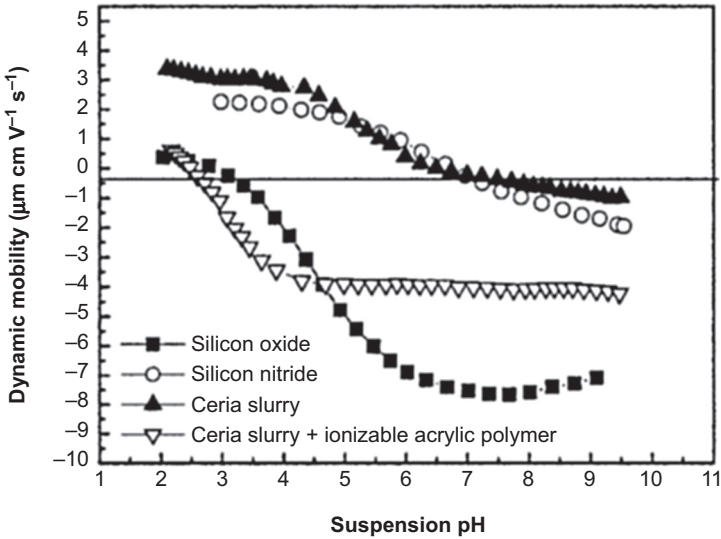

Figure 11.12 Electrokinetic behaviors of SiO_2, Si_3N_4, CeO_2, and CeO_2 with anionic surfactant as a function of suspension pH.
Kim et al. (2003).

high selectivity between SiO_2 and Si_3N_4. Ceria abrasives have the pH_{pzc} at pH 8. With the addition of anionic dispersants, ceria abrasive shows a highly negative charge in the pH range 2.5−11.

The surface charges of ceria are different depending on their synthesis methods (Figure 11.13). Whereas solid-state ceria forms the hydroxyl groups in aqueous media, solution-grown ceria inevitably contains large concentrations of nitrate ions that originate from the precursor such as cerium nitrate (Nabavi et al., 1993). These nitrate ions preferentially adsorb on the surface during synthesis. For this reason, the pH_{pzc} of solid-state ceria and solution-grown ceria are observed at slightly different pH values, 8.3 and 10.4, respectively. Adsorption of specific ions on the abrasive surface can change the surface charge as a function of pH, which modifies their CMP performances. This will be discussed in Section 3.3.3.

In contrast with STI CMP slurries, metal CMP slurries have higher ionic strength because of the addition of oxidizer, inhibitors, and complexing agents. At high ionic strength, counter ions are attracted to the charged interface and form a diffuse ion "cloud" adjacent to the particle surface. Counter ions surrounding the interface of particles reduce the surface charge of the particles through charge screening, which causes agglomeration and settling. Choi et al. studied the effect of ionic strength on CMP (Choi et al., 2004). They observed agglomerations of particle at high ionic strength because surface charge is decreased by the charge screening. Although the agglomerated particles can increase the MRR because of their larger size, they cause significant surface damages on film during polishing.

Figure 11.14 shows the addition of the various surfactants such as CPC (cationic surfactant), SDS (anionic surfactant), and Triton X-100 (nonionic surfactant) in

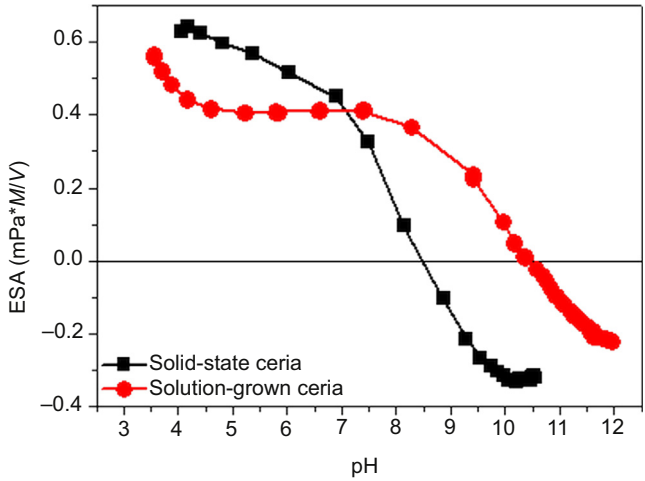

Figure 11.13 Electrokinetic behaviors of solid-state and solution-grown ceria as a function of pH.
Seo et al. (2014).

alumina slurries at high ionic strength (Palla and Shah, 2000). All these slurries show very rapid settling although fractional volume for settling varies with the surfactants. Palla and Shah proposed various strategies to disperse the abrasive particles at high ionic strength (Figure 11.15). They suggested that the slurries with mixed anionic

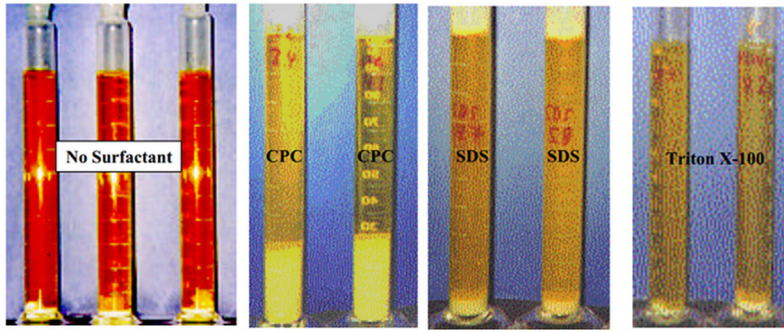

Figure 11.14 Effects of ionic or nonionic surfactant addition on high ionic strength slurry containing 0.1 M potassium ferricyanide oxidizing agent. The slurries are 1 wt% AKP-50 alumina at pH 4 with 10 mM surfactant added. The photographs were taken after 24 h of settling. Palla and Shah (2000).

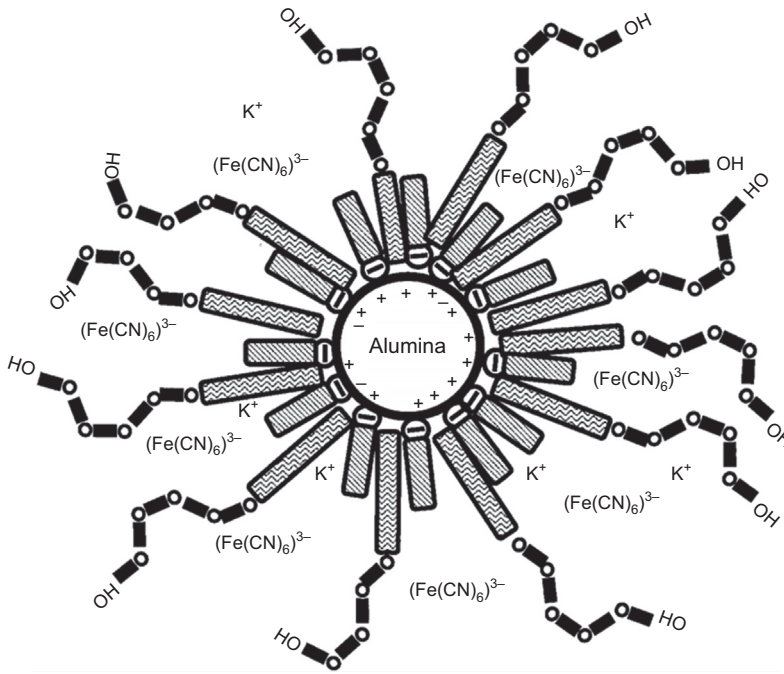

Figure 11.15 Strategy for dispersion stability at high ionic strength. Palla and Shah (2000).

and nonionic surfactants can improve dispersion stability through steric stabilization. The anionic surfactant adsorbs on the alumina abrasive, and the nonionic surfactant interacts with the anionic surfactant. This surfactant structure is not affected by ionic strength.

11.3.3 Surface chemistry

In an aqueous media, abrasive particles are sensitive to the changes in their physico-chemical conditions including pH, ionic strength, temperature, and concentration, which have significant influence on their surface chemistry. Hence, an understanding of the surface chemistry of the abrasive particles is essential for their CMP application. Seo et al. have identified through Fourier-transform infrared spectroscopy (FTIR) that surface functional groups of ceria abrasive varied with synthesis methods (Seo et al., 2014). The −OH groups on the ceria surface can be generated by dissociation reaction of H_2O on the defect site. In general, solid-state ceria forms the −OH groups in aqueous media. However, solution-grown ceria inevitably contains large concentrations of nitrate ions, which originate from the precursor such as cerium nitrate. These nitrate ions were covalently bound on the surface during synthesis, which have an influence on CMP performance. Seo et al. experimentally and theoretically demonstrated the effect of surface functional groups such as $-NO_3$ and −OH groups on CMP performance (Seo et al., 2014). Experimental results derived from adsorption isotherms of silicate ions on ceria surface show the $-NO_3$ group has a much higher affinity with silicate than the −OH group. Theoretical analysis using density functional theory calculation shows that the binding energy of the NO_3-ceria (−4.383 eV) on the SiO_2 surface is much higher than that of the OH-ceria (−3.813 eV) (Figure 11.16). As shown in Figure 11.17, the CMP result shows that the SiO_2 RR of NO_3-ceria (360 nm/min) is higher than that of OH-ceria (274 nm/min). These results imply that surface functional groups of particle surface have a significant influence on CMP performance.

The synthesis methods as well as pH of the reaction medium have significant influence on the surface chemistry of the synthesized materials. Wu et al. reported that the pH of a reaction medium has an influence on the crystallization of ceria under hydrothermal methods (Wu et al., 2002). The result showed that grain growth in acidic medium is faster due to the dissolution rate of precursor than that in alkaline medium. Ceria, synthesized in an acidic medium, has higher Ce^{3+} concentrations on the surface than those synthesized in an alkaline medium. Presumable, it shows high SiO_2 MRR caused by the high Ce^{3+} concentrations.

Abrasive sizes less than 100 nm are extremely sensitive to changes in their physico-chemical environments because of the higher surface energy compared to larger abrasives. The formation of an oxygen vacancy leaves electrons at the surface, which reduces Ce^{4+} to Ce^{3+} ions (Tsunekawa et al., 1999). Figure 11.18 shows lattice parameter as a function of size of ceria. Tsunekawa et al. found through the electron diffraction patterns that small size ceria has higher Ce^{3+} concentrations compared to bulk ceria. They reported that it is attributed to the increased surface-to-volume ratio of the small particle.

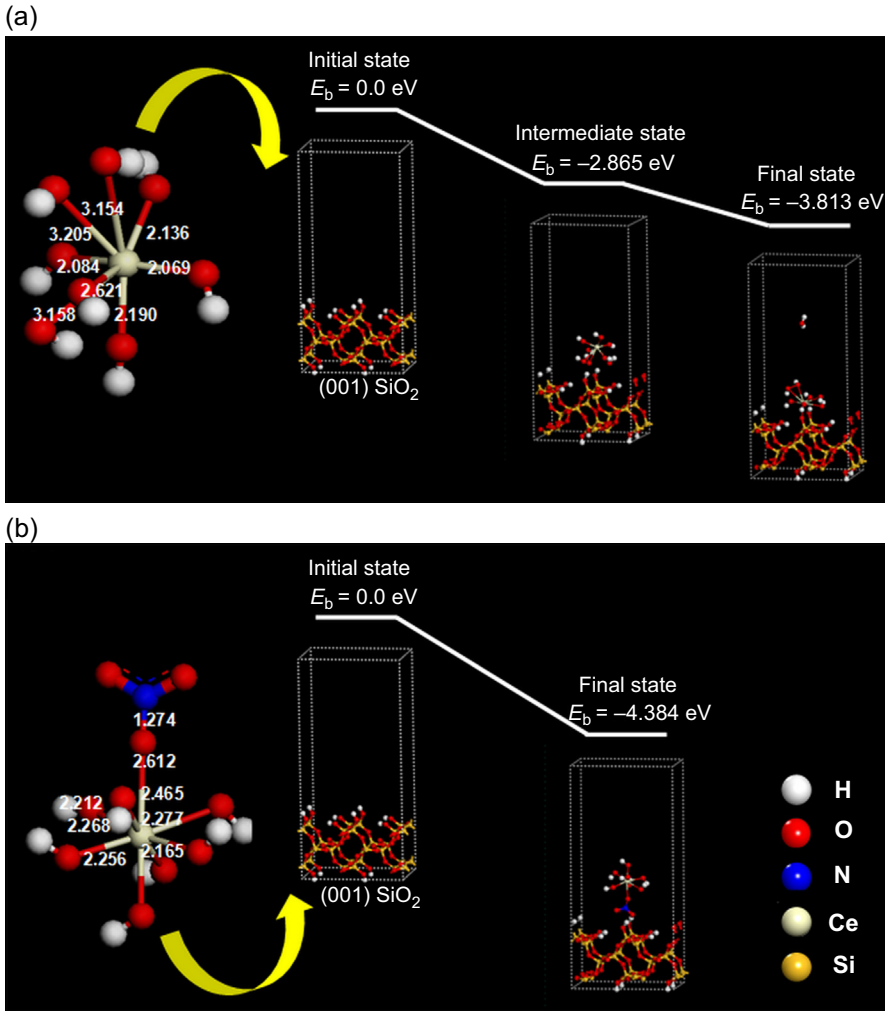

Figure 11.16 Fully optimized structures on the reaction of functionalized ceria adsorption on the SiO_2 (001) surface: (a) OH-ceria and (b) NO_3-ceria. The numbers indicate bonding length of two atoms near to the Ce atom.
Seo et al. (2014).

Surface chemistry of silica also varies with synthesis methods (Zhang et al., 2012). Figure 11.19(a) shows the normalized Raman spectra results of fumed and colloidal silica. Spectral bands at $\sim$600 cm^{-1}, $\sim$490 cm^{-1}, and $\sim$450 cm^{-1} are related to three-, four-, and five-membered siloxane rings, respectively (Brinker et al., 1988). Fumed silica has prominent bands at $\sim$600 cm^{-1}, $\sim$490 cm^{-1}, and $\sim$450 cm^{-1}, while colloidal silica has none at $\sim$600 cm^{-1}. Fumed silica has a structure with an intrinsic population of both strained three-membered rings as well as larger unstrained

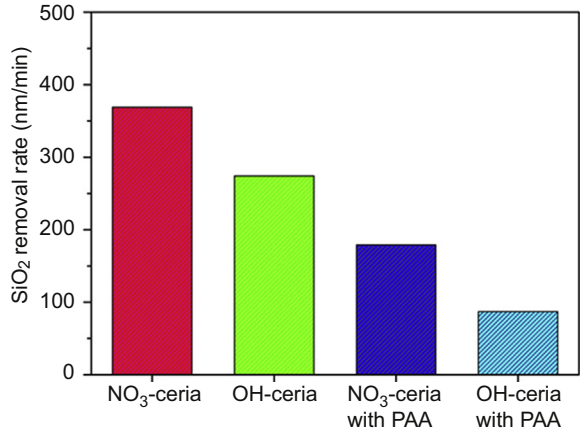

Figure 11.17 Removal rate of SiO_2 film of NO_3-ceria and OH-ceria at pH 7.0. Seo et al. (2014).

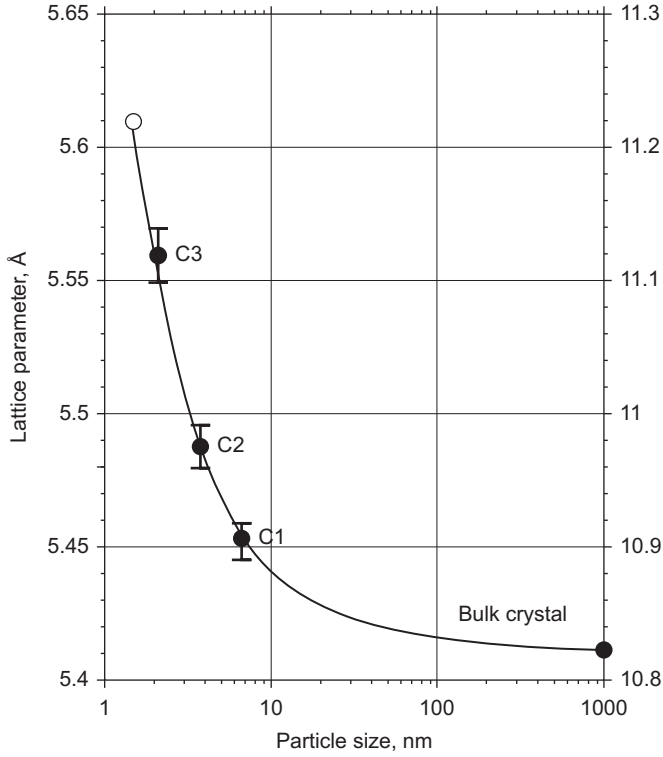

Figure 11.18 Plot of lattice parameters versus particle sizes of three samples and a bulk crystal. Tsunekawa et al. (1999).

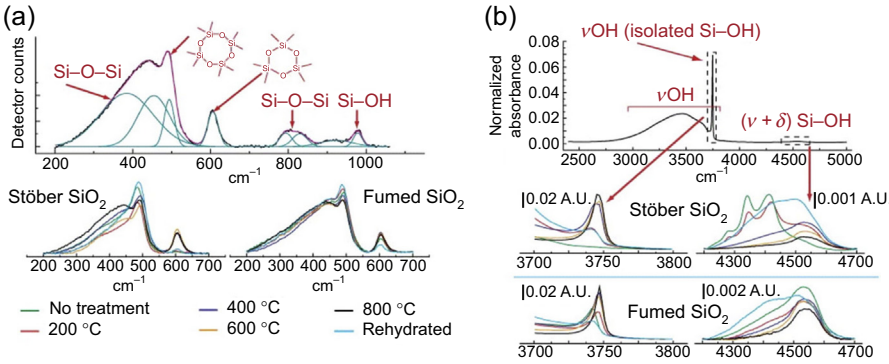

Figure 11.19 Physical and spectroscopic characterization of fumed and colloidal silica nanoparticles: (a) Raman spectroscopy of silica samples used to examine the relative concentration of four- and three-membered ring structures; (b) FTIR analysis of silanol concentration in fumed and colloidal silica using vibrational bands at ~3745 cm^{-1} (nonhydrogen-bonded silanols only) and 4500 cm^{-1} (total silanol population). Zhang et al. (2012).

rings caused by high-temperature synthesis (>1300°C) and rapid thermal quenching. In contrast, colloidal silica structures involved principally unstrained four-membered and larger rings formed by continued condensation reactions. Figure 11.19(b) shows FTIR analysis of silanol concentration in fumed and colloidal silica. Broad peaks at 4500 cm^{-1} are related to the total (hydrogen-bonded and isolated) hydroxyl concentration, and peaks at 3460 cm^{-1} and 3750 cm^{-1} are related to hydrogen-bonded vicinal and isolated silanols, respectively. Fumed silica has a lower total hydroxyl content (2.8 OH/nm^2) and a higher portion of isolated silanol than colloidal silica (4.5 OH/nm^2). These reactive sites on the surface produce ·OH with H_2O_2 or water according to a Fenton-like reaction (Fubini and Hubbard, 2003). The reactivity between silica and H_2O_2 is very important because H_2O_2 has been widely used as oxidants for metal slurries.

Silica abrasives show different surface chemistry as the abrasive size decreases. Kamiya et al. studied the effect of silica size on surface silanol structure through FTIR (Kamiya et al., 2000). For relatively small particles (<10 nm in diameter), the isolated silanol is observed. However, as the particle diameter increased to >30 nm, the surface density of the isolated silanol decreased, and hydrogen-bonded silanol groups are Increased due to the strong hydration force between the silanols. These size-dependent differences of surface chemistry of silica can lead to a variation of surface charge on silica (Puddu and Perry, 2014) (Figure 11.20). With an increase in the particle size, an increase in surface charge is observed. Although there is no report that the effect of surface chemistry varied with particle size on CMP performance, understanding the surface chemistry of abrasive particles is very important because it has a significant influence on CMP performance.

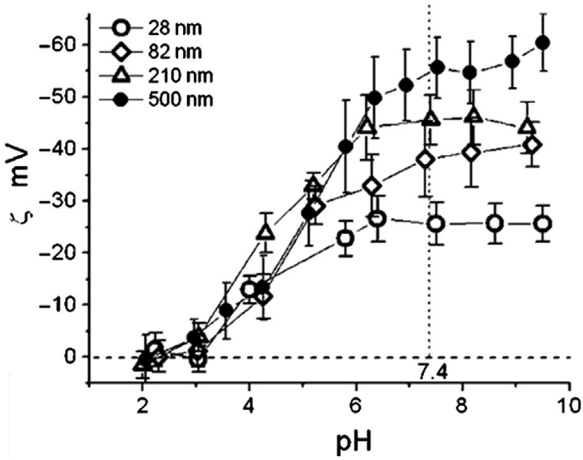

Figure 11.20 Zeta potential of silica nanoparticles as a function of pH. Puddu and Perry (2014).

11.3.4 Rheological behavior

During polishing, CMP slurries are transported into the pores of the polishing pad by high speed rotation. These slurries form a liquid film between the polishing pad and the wafer, which determines the contact regime between them. Figure 11.21 is the coefficient of friction (COF) as a function of a lubrication parameter ($\eta V/P$), which is known as the Stribeck curve; it shows three distinct regions: boundary lubrication, mixed lubrication, and hydrodynamic lubrication (Philipossian and Olsen, 2003). Boundary lubrication is dominated by solid−solid contact. In this regime, the COF shows a high value because of direct contact between the solid surfaces. However, the COF is not

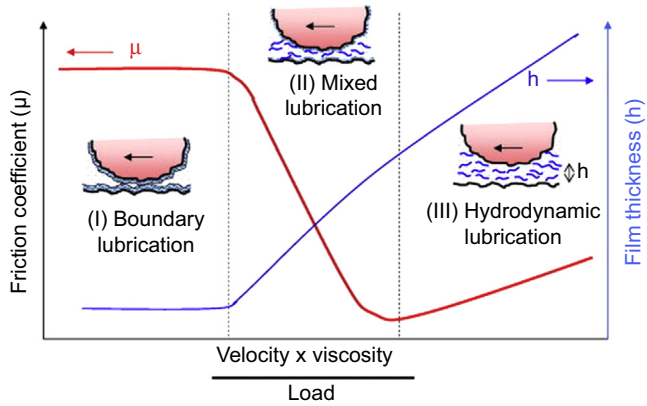

Figure 11.21 Friction coefficient plotted as a function of fluid viscosity and shear velocity divided by load (Stribeck curve) with corresponding lubrication film thickness. Coles et al. (2010).

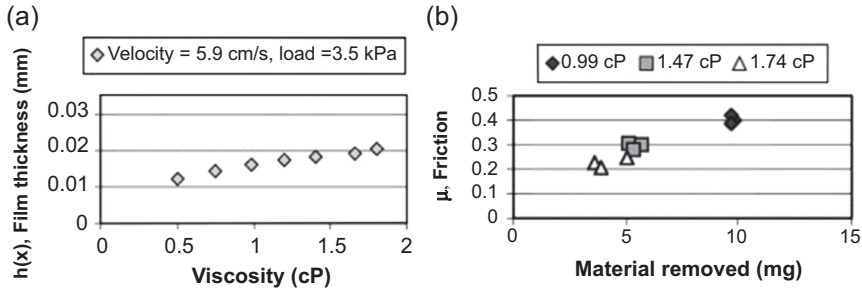

Figure 11.22 (a) The thickness of lubrication film as a function of slurry viscosity and (b) the COF against MRR depending on slurry viscosity (velocity = 12.6 cm/s, pressure = 3.5 kPa). Mullany and Byrne (2003).

significantly changed despite an increase in the lubrication parameter. The second region is known as partial lubrication, where the liquid film formed between the pad and wafer is more important and the COF decreases with an increase in the lubrication parameter. The third region is hydrodynamic lubrication, which shows the low COF value. The pad and wafer are fully separated because of the formation of thick liquid film. The COF increases slightly with an increase in the lubrication parameter. Mullany and Byrne experimentally and theoretically investigated the effect of slurry viscosity on MRR (Mullany and Byrne, 2003). As viscosity is increased while other variables such as velocity and pressure were kept constant, the thickness of liquid film is greater (Figure 11.22(a)). This thick liquid film decreases the COF value, resulting in a decrease in MRR (Figure 11.22(b)). The COF against the lubrication parameter shows a downward slope. Thus, they suggested that the experiment was processed in the partial lubrication region.

11.4 Conclusion

In this chapter, we described the role of each component in CMP slurry, and discussed the characterization of slurries for CMP. Since CMP was developed in the 1980s, many researchers have investigated CMP slurries in a variety of ways. However, there is still a need to understand more profoundly how the slurry characteristics affect CMP performance. These issues can be solved through a fundamental study of powder technology, surface chemistry, and colloidal chemistry.

References

Asakura, S., Oosawa, F., 1954. On interaction between two bodies immersed in a solution of macromolecules. J. Chem. Phys. 22, 1255−1256.

Asakura, S., Oosawa, F., 1958. Interaction between particles suspended in solutions of macromolecules. J. Polym. Sci. 33, 183−192.

Basim, G.B., Adler, J.J., Mahajan, U., Singh, R.K., Moudgil, B.M., 2000. Effect of particle size of chemical mechanical polishing slurries for enhanced polishing with minimal defects. J. Electrochem. Soc. 147, 3523−3528.

Basim, G.B., Vakarelski, I.U., Moudgil, B.M., 2003. Role of interaction forces in controlling the stability and polishing performance of CMP slurries. J. Colloid Interface Sci. 263, 506−515.

Beyer, K.D., 1999. A "Dirty" Risk. In: Innovative Leader. 8, 407.

Bielmann, M., Mahajan, U., Singh, R.K., 1999. Effect of particle size during tungsten chemical mechanical polishing. Electrochem. Solid State Lett. 2, 401−403.

Bokare, A.D., Choi, W., 2014. Review of iron-free Fenton-like systems for activating H_2O_2 in advanced oxidation processes. J. Hazard. Mater. 275, 121−135.

Brinker, C., Kirkpatrick, R., Tallant, D., Bunker, B., Montez, B., 1988. NMR confirmation of strained "defects" in amorphous silica. J. Non-Cryst. Solids 99, 418−428.

Bu, K.-H., Moudgil, B.M., 2007. Selective chemical mechanical polishing using surfactants. J. Electrochem. Soc. 154, H631−H635.

Choi, W., Lee, S.-M., Singh, R.K., 2004. pH and down load effects on silicon dioxide dielectric CMP. Electrochem. Solid-State Lett. 7, G141−G144.

Coles, J.M., Chang, D.P., Zauscher, S., 2010. Molecular mechanisms of aqueous boundary lubrication by mucinous glycoproteins. Curr. Opin. Colloid Interface Sci. 15, 406−416.

Cook, L.M., 1990. Chemical processes in glass polishing. J. Non-Cryst. Solids 120, 152−171.

Cui, H., Park, J.-H., Park, J.-G., 2013. Effect of oxidizers on chemical mechanical planarization of ruthenium with colloidal silica based slurry. ECS J. Solid State Sci. Technol. 2, P26−P30.

Dandu, P.R.V., Peethala, B.C., Amanapu, H.P., Babu, S.V., 2011. Silicon nitride film removal during chemical mechanical polishing using ceria-based dispersions. J. Electrochem. Soc. 158, H763−H767.

Dandu, P.R.V., Peethala, B.C., Babu, S.V., 2010. Role of different additives on silicon dioxide film removal rate during chemical mechanical polishing using ceria-based dispersions. J. Electrochem. Soc. 157, Ii869−Ii874.

Derjaguin, B.V., Landau, L.D., 1941. Theory of the stability of strongly charged lyophobic sols and of the adhesion of strongly charged particles in solutions of electrolytes. Acta Phys. Chim. 14, 633−662.

Du, T., Luo, Y., Desai, V., 2004. The combinatorial effect of complexing agent and inhibitor on chemical−mechanical planarization of copper. Microelectron. Eng. 71, 90−97.

Ein-Eli, Y., Abelev, E., Rabkin, E., Starosvetsky, D., 2003. The compatibility of copper CMP slurries with CMP requirements. J. Electrochem. Soc. 150, C646−C652.

Fubini, B., Hubbard, A., 2003. Reactive oxygen species (ROS) and reactive nitrogen species (RNS) generation by silica in inflammation and fibrosis. Free Radic. Biol. Med. 34, 1507−1516.

Hackley, V.A., 1997. Colloidal processing of silicon nitride with poly(acrylic acid). 1. Adsorption and electrostatic interactions. J. Am. Ceram. Soc. 80, 2315−2325.

Kamiya, H., Mitsui, M., Takano, H., Miyazawa, S., 2000. Influence of particle diameter on surface silanol structure, hydration forces, and aggregation behavior of alkoxide-derived silica particles. J. Am. Ceram. Soc. 83, 287−293.

Kaufman, F., Thompson, D., Broadie, R., Jaso, M., Guthrie, W., Pearson, D., Small, M., 1991. Chemical-Mechanical polishing for fabricating patterned W metal features as chip interconnects. J. Electrochem. Soc. 138, 3460−3465.

Kelsall, A., 1998. Cerium oxide as a mute to acid free polishing. Glass Technol. 39, 6−9.

Kim, D.-H., Kang, H.-G., Kim, S.-K., Paik, U., Park, J.-G., 2006. Reduction of large particles in ceria slurry by aging and selective sedimentation and its effect on shallow trench isolation chemical mechanical planarization. Jpn. J. Appl. Phys. 45, 6790.

Kim, H.M., Venkatesh, R.P., Kwon, T.Y., Park, J.G., 2012. Influence of anionic polyelectrolyte addition on ceria dispersion behavior for quartz chemical mechanical polishing. Colloids Surf. Physicochem. Eng. Aspects 411, 122−128.

Kim, S.K., Lee, S., Paik, U., Katoh, T., Park, J.G., 2003. Influence of the electrokinetic behaviors of abrasive ceria particles and the deposited plasma-enhanced tetraethylorthosilicate and chemically vapor deposited Si_3N_4 films in an aqueous medium on chemical mechanical planarization for shallow trench isolation. J. Mater. Res. 18, 2163−2169.

Kim, Y.H., Kim, S.K., Park, J.G., Paik, U., 2010. Increase in the adsorption density of anionic molecules on ceria for defect-free STI CMP. J. Electrochem. Soc. 157, H72−H77.

Kim, Y.H., Lee, S.M., Lee, K.J., Paik, U., Park, J.G., 2008. Constraints on removal of Si_3N_4 film with conformation-controlled poly(acrylic acid) in shallow-trench isolation chemical-mechanical planarization (STI CMP). J. Mater. Res. 23, 49−54.

Krishnan, M., Nalaskowski, J.W., Cook, L.M., 2009. Chemical mechanical planarization: slurry chemistry, materials, and mechanisms. Chem. Rev. 110, 178−204.

Kurokawa, S., Doi, T., Ohnishi, O., Yamazaki, T., Tan, Z., Yin, T., 2013. Characteristics in SiC-CMP using MnO_2 slurry with strong oxidant under different atmospheric conditions. MRS Proc. Cambridge Univ Press, mrss13-1560-bb03-01.

Lee, H., Joo, S., Jeong, H., 2009. Mechanical effect of colloidal silica in copper chemical mechanical planarization. J. Mater. Process. Technol. 209, 6134−6139.

Lee, J.D., Park, Y.R., Yoon, B.U., Han, Y.P., Hah, S., Moon, J.T., 2002. Effects of nonionic surfactants on oxide-to-polysilicon selectivity during chemical mechanical polishing. J. Electrochem. Soc. 149, G477−G481.

Lei, H., Luo, J., 2004. CMP of hard disk substrate using a colloidal SiO_2 slurry: preliminary experimental investigation. Wear 257, 461−470.

Lei, H., Zhang, P., 2007. Preparation of alumina/silica core-shell abrasives and their CMP behavior. Appl. Surf. Sci. 253, 8754−8761.

Lim, J.-H., Park, J.-H., Park, J.-G., 2013. Effect of iron (III) nitrate concentration on tungsten chemical-mechanical-planarization performance. Appl. Surf. Sci. 282, 512−517.

Luo, J., Dornfeld, D.A., 2003. Material removal regions in chemical mechanical planarization for submicron integrated circuit fabrication: coupling effects of slurry chemicals, abrasive size distribution, and wafer-pad contact area. IEEE Trans. Semicond. Manuf. 16, 45−56.

Mullany, B., Byrne, G., 2003. The effect of slurry viscosity on chemical−mechanical polishing of silicon wafers. J. Mater. Process. Technol. 132, 28−34.

Nabavi, M., Spalla, O., Cabane, B., 1993. Surface-chemistry of nanometric ceria particles in aqueous dispersions. J. Colloid Interface Sci. 160, 459−471.

Notoya, T., Poling, G.W., 1976. Topographies of thick Cu-benzotriazolate films on copper. Corrosion 32, 216−223.

Paik, U., Kim, J., Jung, Y., Jung, Y., Katoh, T., Park, J., Hackley, V., 2001. The effect of Si dissolution on the stability of silica particles and its influence on chemical mechanical polishing for interlayer dielectric. J. Korean Phys. Soc. 39, S201−S204.

Palla, B.J., Shah, D.O., 2000. Stabilization of high ionic strength slurries using the synergistic effects of a mixed surfactant system. J. Colloid Interface Sci. 223, 102−111.

Park, J.-G., Katoh, T., Lee, W.-M., Jeon, H., Paik, U., 2003. Surfactant effect on oxide-to-nitride removal selectivity of nano-abrasive ceria slurry for chemical mechanical polishing. Jpn. J. Appl. Phys. 42, 5420.

Penta, N.K., Amanapu, H.P., Peethala, B.C., Babu, S.V., 2013a. Use of anionic surfactants for selective polishing of silicon dioxide over silicon nitride films using colloidal silica-based slurries. Appl. Surf. Sci. 283, 986–992.

Penta, N.K., Peethala, B.C., Amanapu, H.P., Melman, A., Babu, S.V., 2013b. Role of hydrogen bonding on the adsorption of several amino acids on SiO_2 and Si_3N_4 and selective polishing of these materials using ceria dispersions. Colloids Surf. A: Physicochem. Eng. Aspects 429, 67–73.

Pettersson, A., Marino, G., Pursiheimo, A., Rosenholm, J.B., 2000. Electrosteric stabilization of Al_2O_3, ZrO_2, and 3Y-ZrO_2 suspensions: effect of dissociation and type of polyelectrolyte. J. Colloid Interface Sci. 228, 73–81.

Philipossian, A., Olsen, S., 2003. Fundamental tribological and removal rate studies of inter-layer dielectric chemical mechanical planarization. Jpn. J. Appl. Phys. 42, 6371.

Puddu, V., Perry, C.C., 2014. Interactions at the silica-peptide interface: the influence of particle size and surface functionality. Langmuir 30, 227–233.

Remsen, E.E., Anjur, S., Boldridge, D., Kamiti, M., Li, S., Johns, T., Dowell, C., Kasthurirangan, J., Feeney, P., 2006. Analysis of large particle count in fumed silica slurries and its correlation with scratch defects generated by CMP. J. Electrochem. Soc. 153, G453–G461.

Remsen, E.E., Anjur, S.P., Boldridge, D., Kamiti, M., Li, S., 2005. Correlation of defects on dielectric surfaces with large particle counts in chemical-mechanical planarization (CMP) slurries using a new single particle optical sensing (SPOS) technique. MRS Proc. Cambridge Univ Press.

Sehgal, A., Lalatonne, Y., Berret, J.F., Morvan, M., 2005. Precipitation-redispersion of cerium oxide nanoparticles with poly(acrylic acid): toward stable dispersions. Langmuir 21, 9359–9364.

Seo, J., Lee, J.W., Moon, J., Sigmund, W.M., Paik, U., 2014. The role of surface chemistry of ceria surfaces on the silicate adsorption. ACS Appl. Mater. Interfaces 6, 7388–7394.

Sigmund, W.M., Bell, N.S., Bergstr, M.L., 2000. Novel powder-processing methods for advanced ceramics. J. Am. Ceramic Soc. 83, 1557–1574.

Tamboli, D., Banerjee, G., Waddell, M., 2004. Novel interpretations of CMP removal rate dependencies on slurry particle size and concentration. Electrochem. Solid State Lett. 7, F62–F65.

Tsunekawa, S., Sivamohan, R., Ito, S., Kasuya, A., Fukuda, T., 1999. Structural study on monosize CeO_2-x nano-particles. Nanostruct. Mater. 11, 141–147.

Veera, P.D., Natarajan, A., Hegde, S., Babu, S., 2009. Selective polishing of polysilicon during fabrication of microelectromechanical systems devices. J. Electrochem. Soc. 156, H487–H494.

Verwey, E.J.W., Overbeek, J.T.G., Overbeek, J.T.G., 1999. Theory of the Stability of Lyophobic Colloids. Courier Dover Publications.

Wang, L., Zhang, K., Song, Z., Feng, S., 2007. Ceria concentration effect on chemical mechanical polishing of optical glass. Appl. Surf. Sci. 253, 4951–4954.

Wu, N.C., Shi, E.W., Zheng, Y.Q., Li, W.J., 2002. Effect of pH of medium on hydrothermal synthesis of nanocrystalline cerium(IV) oxide powders. J. Am. Ceramic Soc. 85, 2462–2468.

Zhang, H., Dunphy, D.R., Jiang, X., Meng, H., Sun, B., Tarn, D., Xue, M., Wang, X., Lin, S., Ji, Z., 2012. Processing pathway dependence of amorphous silica nanoparticle toxicity: colloidal vs pyrolytic. J. Am. Chem. Soc. 134, 15790–15804.

Zhang, Z., Lei, H., 2008. Preparation of α-alumina/polymethacrylic acid composite abrasive and its CMP performance on glass substrate. Microelectron. Eng. 85, 714–720.